Nanoscale

Accepted Manuscript

Cite this: DOI: 10.1039/c0xx00000x

www.rsc.org/xxxxxx

ARTICLE TYPE

$Bi_xLa_{1-x}VO_4$ Solid Solutions: Tuning of Electronic Properties via Stoichiometry Modifications

Przemysław Kwolek,[a] Kacper Pilarczyk,[b,d] Tomasz Tokarski,[a] Kornelia Lewandowska,[a,c] Konrad Szaciłowski,[a,d]*

Received (in XXX, XXX) XthXXXXXXXXX 20XX, Accepted Xth XXXXXXXXX 20XX
DOI: 10.1039/b000000x

Dedicated to professor Krzysztof Fitzner on the occasion of his 70th birthday

$Bi_xLa_{1-x}VO_4$ solid solutions were obtained in the form of fine powder via a microwave-assisted hydrothermal route. The presence of a solid solution in the studied system was confirmed using X-ray diffraction technique (XRD) and optical spectroscopy. Pure $BiVO_4$ and $LaVO_4$ were obtained in the monoclinic form, whereas solid solutions in the tetragonal, zircon-type structure. The optical band gap dependence on a composition of the solid solution is parabolic, thus there is a possibility to tune this parameter in a wide concentration range, from 2.4 to 4.0 eV. An absorption coefficient maximum is also concentration-dependent, possibly, due to the structural disorder of the samples. Between 11.94 and 32.57 at. % of Bi^{3+} concentration, solid solutions exhibit intense, green luminescence. It indicates the presence of Bi-originated electronic states within the band gap. A value of the conduction band edge potential, measured both with an electrochemical impedance spectroscopy and work function measurements, is concentration-independent. Moreover, solid solutions exhibit a Photoelectrochemical Photocurrent Switching Effect, thus they may be promising materials for molecular electronics and dioxygen activator.

Introduction

Bismuth orthovanadate is a very promising material with potential use in several fields. To begin with, it is commercially used in the pigment industry,[1] at the same time, it is also a very promising photocatalyst for O_2 evolution in photoelectrochemical cells, as well as for degradation of organic pollutants from wastewater.[2] In the Earth crust, $BiVO_4$ occurs in the orthorhombic crystal structure (pucherite).[3] There are also other known polymorphs, namely: monoclinic (*m*$BiVO_4$, clinobisvanite), exhibiting the best photocatalytic activity, tetragonal scheelite-like (*st*$BiVO_4$, high temperature phase) and tetragonal, zircon-type (*zt*$BiVO_4$, dreyerite).[4] $BiVO_4$ is the an *n*-type semiconductor with a value of the band gap varying for different polymorphs. Both *m*$BiVO_4$ and *st*$BiVO_4$ have similar band gaps (2.4 and 2.3 eV respectively).[5, 6] *zt*$BiVO_4$ in turn, has a wider band gap, equal to 2.9 eV.[6] The electronic structures of *m*$BiVO_4$ and *st*$BiVO_4$ phases are quite similar. The valence bands are dominated by oxygen 2*p* states with some contribution of bismuth 6*s* states, which are located close to the valence band edge. For *zt*$BiVO_4$ polymorph, stronger interaction between O 2*p* and Bi 6*s* states occurs. Conduction bands, in turn, are composed mainly of vanadium 3*d* states with significant contributions of O 2*p* and Bi 6*p* levels. Both *m*$BiVO_4$ and *st*$BiVO_4$ are indirect band gap semiconductors, whereas, for *zt*$BiVO_4$, the DFT calculations indicated the predominance of the direct transition.[7, 8]

Pure lanthanum orthovanadate is much less frequently applied as a photocatalyst,[9] however, it may be a good candidate for catalyst in the oxidation of NH_3 to NO and H_2S to the elemental sulphur.[10, 11] It is also considered as a promising host for luminescent lanthanide ions.[12] Lanthanum orthovanadate crystallizes in two polymorphs, namely monazite-type monoclinic (*m*$LaVO_4$) and zircon-type, tetragonal (*zt*$LaVO_4$), which is a metastable phase.[13, 14] The upper parts of the valence bands in the vicinity of the band maxima, for both $LaVO_4$ polymorphs are composed mainly of O 2*p* and V 3*d* states, with a small contribution of La 5*d* states. The lower parts of the conduction bands, slightly above the band edges, are also composed of O 2*p* and V 3*d* states, with a La 6*p* admixture (more prominent in the case of *zt*$LaVO_4$). Whereas O 2*p* dominates the valence band, the V 3*d* states are the major component of the conduction band. The interband transition in *m*$LaVO_4$, similarly to *m*$BiVO_4$, is indirect, whereas in *zt*$LaVO_4$ is direct as in *zt*$BiVO_4$.[14] The band gap energy for *m*$LaVO_4$ is equal to 3.5 eV.[15] Although *zt*$LaVO_4$ has been successfully synthesised,[16-18] the band gap has not been determined yet. The value obtained using DFT calculations equals to 3.01 eV,[14] however, this method is known to give underestimated results. The band gap of *m*$LaVO_4$ was calculated as equal to 3.42 eV, which is slightly below the measured value of 3.5 eV.[14]

The cation substitution is a very common way for modifying both the band gap energy and the band edge potentials. In general, substitution of an electropositive cation, exhibiting noble gas

configuration (like La^{3+}) with a *p*-block cation (like Bi^{3+}) should decrease the value of the band gap.[19] The more similar ionic radii are, the wider range of solubility is. For $BiVO_4$ – $LaVO_4$ system, ionic radii are 115 pm for La^{3+} and 103 pm for Bi^{3+}.[20] These values indicate the possibility of substitution of La^{3+} ion with Bi^{3+}, while retaining the lattice symmetry. Common crystal structure, (tetragonal, zircon type), the same valency and similar electronegativity values of both cations should also extend the range of solubility.[21]

On the whole, $BiVO_4$ as well as $LaVO_4$ are obtained by the solvothermal (in particular hydrothermal) route[16-18, 22, 23] or solid state reactions.[24, 25] A microwave-assisted method of synthesis can also be applied.[15, 26]

Although vanadates are extensively examined due to their promising properties, the $BiVO_4$ – $LaVO_4$ system has not been paid much attention yet. So far, only its photocatalytic activity was investigated.[20] We hypothesize that the electronic and photoelectrochemical properties of the $Bi_xLa_{1-x}VO_4$ solid solutions can be tuned via stoichiometry modifications. Therefore, detailed study on the synthesis, structure and electronic properties of these materials was undertaken. To authors best knowledge, there are no reports on the synthesis of these solid solutions in such a wide range of composition.

Experimental

The synthesis was performed in a microwave heated, high pressure autoclave Magnum II (*Ertec*, Poland). Bismuth nitrate ($Bi(NO_3)_3{\cdot}5H_2O$, *Sigma Aldrich*, 98.5%) and lanthanum nitrate ($La(NO_3)_3{\cdot}6H_2O$, *Alfa Aesar*, 99.99%) were dissolved in 20 ml of deionized water and mixed with 5 ml of 2 M HNO_3, which was added to prevent hydrolysis. Sodium orthovanadate was dissolved in 20 ml of deionized water with the addition of 4 ml of 2 M NaOH. Upon mixing of both solutions, pH was adjusted to 7, deionized water was added up to 50 ml and the reaction mixture was transferred into a Teflon vessel. In each case the synthesis was calculated to obtain 1 mmol of the product with the content of $BiVO_4$ varying from 0 to 100 at. % with 10 at. % step. The reaction vessel was tightly sealed in the autoclave and the reaction mixture was heated by a microwave irradiation up to 553 K and kept at this temperature for 1 hour under the pressure of 43 to 45 bar. The precipitate was obtained in the form of a very fine powder, washed several times with deionized water, centrifuged and dried in the air.

The preliminary evidence of samples composition was provided by the results of the inductively coupled plasma atomic emission spectroscopy (ICP-AES) measurements, using the ELAN 6100 spectrometer (*Perkin Elmer*, USA). The samples were prepared by dissolution of approximately 0.003 g of the powder in the concentrated hydrochloric acid. The mixtures were further diluted by the addition of deionized water up to 250 ml. These were examined for the amount of bismuth, lanthanum and vanadium, which allowed to determine the elemental composition of the obtained materials. The crystalline phases were identified by the X-ray diffraction (XRD) technique using the Miniflex II (*Rigaku*, Japan) diffractometer with Cu K_α emission line, λ=0.15406 nm. The morphology of the product was studied with the scanning electron microscopy (SEM) on the SU 70 instrument (*Hitachi*, Japan). The electronic structure of the obtained materials was determined using the diffuse reflectance spectroscopy, fluorescence spectroscopy and electrochemical impedance spectroscopy (EIS) as well as the work function measurements (Kelvin probe, KP technique). Diffuse reflectance spectra were recorded on the Lambda 950 (*Perkin Elmer*, USA) spectrophotometer equipped with the 150 mm integration sphere. 0.01 g of each sample was dispersed in spectrally pure $BaSO_4$ in 1:80 weight ratio. Pressed $BaSO_4$ pellet was used as a reference. Photoluminescence spectra were recorded on the Fluoromax 4P spectrofluorimeter (*Horiba Jobin Yvon*, France). The samples were prepared as follows: 0.002 g of the sample was dispersed in 4 ml of deionized water, then diluted 50 times and homogenized using an ultrasonic bath just before the measurement. The samples were excited at 300 nm. The band edge potentials and work function values of the samples as functions of their composition were estimated according to the results obtained from the EIS and KP respectively. Electrochemical impedance spectra were measured in 0.1 M KCl on the SP-300 potentiostat (*Bio-Logic*, France) *vs.* Ag/AgCl reference electrode. The electrodes for the EIS and KP were prepared by the deposition of the obtained powders onto the indium-tin oxide coated polyethylene terephthalate foil (ITO@PET). The work function values were measured on the ambient Kelvin probe system KP020 (*KP Technology*, Scotland) customized by *Instytut Fotonowy* (Poland). The last step in the characterization of the obtained materials were photoelectrochemical experiments (pulsed photocurrent spectroscopy) performed using a custom-built photoelectric spectrometer (*Instytut Fotonowy*, Poland) equipped with the 150 W xenon arc lamp and coupled with the SP-300 potentiostat. The experiments were performed in 0.1 M KNO_3 *vs.* Ag/AgCl sat. reference electrode.

Results and discussion

The first step after the synthesis was to confirm the elemental content and to determine the phase composition of the obtained materials using ICP-AES and XRD analysis, respectively. ICP-AES measurements indicate a significant deviation of samples composition from the intended ones (Table 1). This may be a result of slightly higher stability/lower solubility of bismuth-rich phases.

Table 1. Assumed and real composition of $Bi_xLa_{1-x}VO_4$ solid solutions.

$BiVO_4$ assumed content [% at.]	$BiVO_4$ real content [% at.]
0	0.00
10	11.94
20	23.47
30	32.57
40	47.75
50	56.97
60	70.80
70	76.48
80	80.75
90	92.86
100	99.80

The XRD diffractograms recorded for all samples are presented in Fig. 1. They reveal that pure $LaVO_4$ exists in the monoclinic crystal structure (space group P21/n (14)), whereas introduction of 11.94 at. % of Bi^{3+} to the material induces the phase transition into the tetragonal, zircon-type structure (space group I41/amd (141)). This transition, however, is incomplete and there are still some remains of the *m*$LaVO_4$ phase, which can be noticed in the

diffraction pattern. This is probably caused by too short hydrothermal treatment of the reaction mixture.

For 11.94 at. % of Bi^{3+}, the observed contribution of the monoclinic phase is significant, for the next sample it considerably decreases and from 32.57 up to 80.75 at. % of Bi^{3+} it is insubstantial. At 92.86 at. % of Bi^{3+}, three different phases exist, namely some remains of mLaVO$_4$, ztBiVO$_4$ and mBiVO$_4$.

□ mBiVO$_4$ space group: I2/b(15) ◊ mLaVO$_4$ space group: P21/n(14)

○ ztLaVO$_4$ (ztBiVO$_4$) space group: I41/amd(141)

Fig. 1. XRD diffractograms for the $Bi_xLa_{1-x}VO_4$ samples.

For pure $BiVO_4$, the monoclinic crystal structure I2/b (15) was obtained. Although it was originally reported for *m*$BiVO_4$, it is a non-standard space group and can be converted to the standard space group C2/c.[27]

These results can be easily explained. Taking into consideration all possible polymorphs of bismuth and lanthanum orthovanadates, only the zircon-type, tetragonal structure is common for both materials. Therefore, introduction of Bi^{3+} into the $LaVO_4$ lattice (or La^{3+} into the $BiVO_4$ lattice), results in the transition from the monoclinic to the tetragonal, zircon-type crystal structure, which in turn suggests the formation of $BiVO_4$ – $LaVO_4$ solid solution. It may be proved by the analysis of the obtained diffraction patterns. It can be seen that increasing Bi^{3+} content results in the alteration of the peak positions, towards the higher values of 2θ angle. At the same time, the higher the value is, the stronger the displacement is. For four most intensive peaks observed for the zircon-type structure (*i.e.* (200), (112), (312) and (332)) the interplanar spacing d_{hkl} was calculated, according to the Bragg's law, Equation (1):

$$d_{hkl} = \frac{\lambda}{2\sin\theta_{hkl}} \quad (1)$$

where λ = 0.15406 nm and θ_{hkl} is the angle, at which the peak originating from the *(hkl)* plane was observed. Subsequently, the parameters *a* and *c* of the tetragonal unit cell were calculated as follows, Equation (2):[28]

$$\frac{1}{d_{hkl}^{\ 2}} = \frac{h^2 + k^2}{a^2} + \frac{l^2}{c^2} \quad (2)$$

The parameter *a* was calculated from the d_{200} interplanar spacing and the *c* values were obtained from the d_{112}, d_{312} and d_{332}. Then, knowing the parameters *a* and *c*, the unit cell volume was estimated. Its changes, in respect to the volume obtained for the sample synthesized with 11.94 at. % of Bi^{3+}, are plotted against the Bi^{3+} content (Fig. 2).

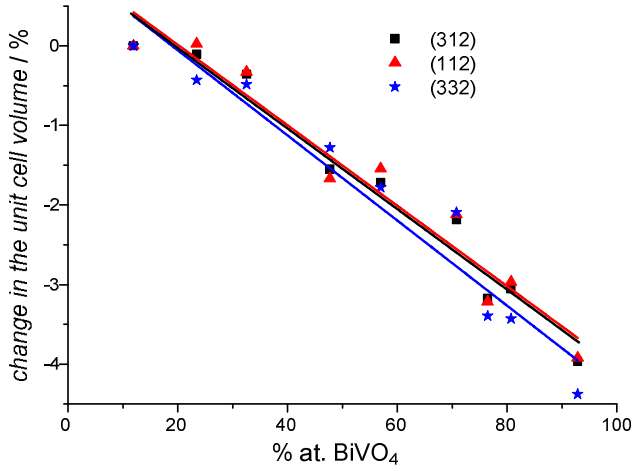

Fig. 2. The change in the unit cell volume (in respect to the 11.94 at. % of Bi^{3+} sample) plotted against Bi^{3+} concentration. The calculations were performed for three different diffraction peaks.

Obtained results clearly indicate that, between 11.94 and 92.86 at. % of Bi^{3+} content, the solid solution was obtained, as the introduction of the bismuth ions into *zt*$LaVO_4$ results in the linear decrease in the unit cell volume. Thus, the $BiVO_4$ – $LaVO_4$ system obeys Vegard's law[29, 30] as the linear dependence of the cell volume versus the composition was found. This indicates a significant ionic character of the lattice,[31] as more covalent semiconductor solid solutions suffer from the significant parabolic deviations from Vegard's law.[32, 33]

The SEM images confirmed the presence of a mixture of at least two phases only for the sample obtained at 92.86 at. % of Bi^{3+} (Fig. 3). Since the *m*$LaVO_4$ phase was obtained in the nanocrystalline form, with the average size below 80 nm, it cannot be observed in the presented SEM image. Moreover, the admixture of this phase is rather insignificant. Therefore, only *m*$BiVO_4$ (regularly-shaped microcrystals) and zircon-type tetragonal phase (nanocrystals) may be distinguished in the SEM image.

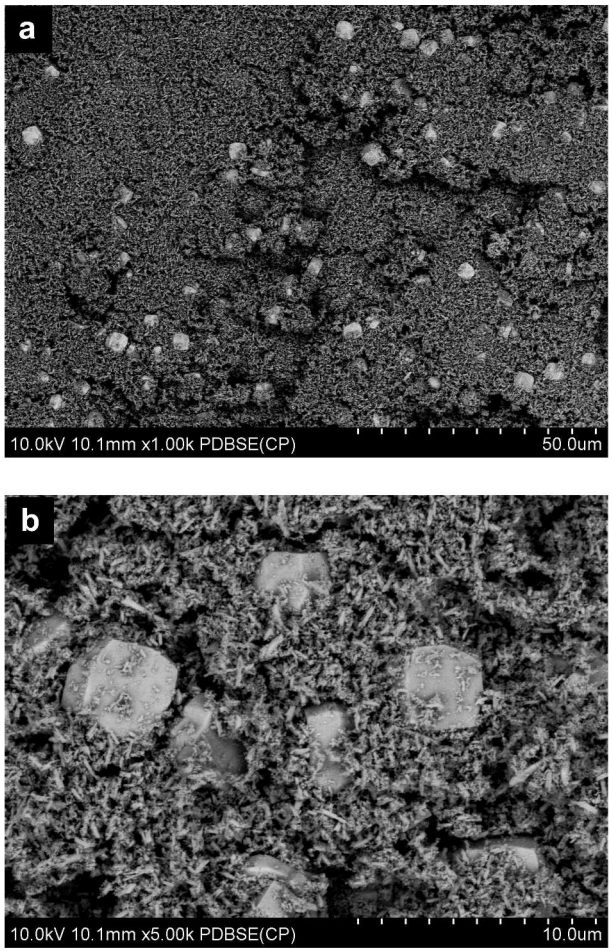

Fig. 3 Morphology of the sample containing 92.86 at. % of Bi^{3+}, characterised by the presence of two phases: Bi – rich (regularly shaped microcrystals) and $BiVO_4$ – $LaVO_4$ solid solution (nanocrystals).

The diffuse reflectance spectroscopy was applied in order to determine the band gaps E_g of the powdery samples. Kubelka-Munk function values f^{KM} were calculated from the normalized reflectance spectra as follows, Equation (3):[34]

$$f^{KM} = \frac{(1-R(h\nu))^2}{2R(h\nu)} = \frac{\alpha(h\nu)}{S} \quad (3)$$

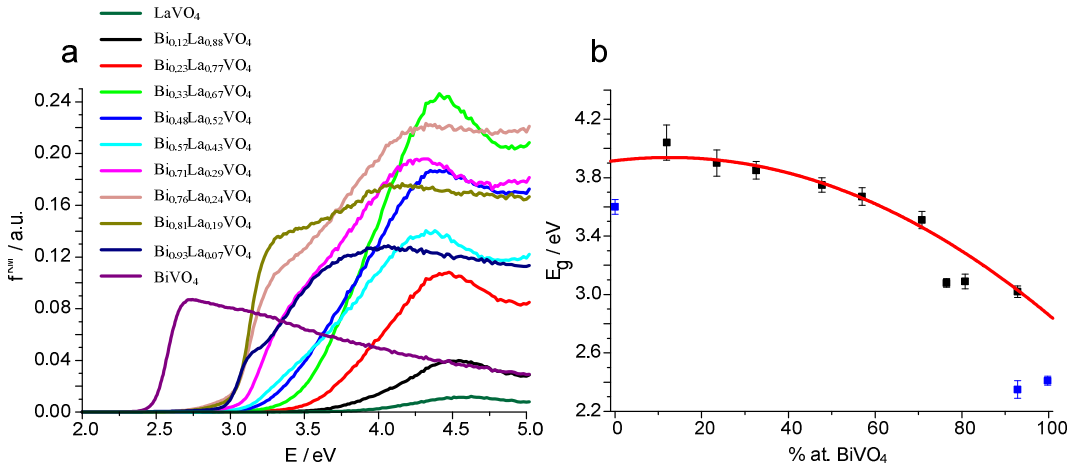

Fig. 4. The absorption spectra (a) and the band gap dependence on the ICP-AES measured composition of the obtained materials (b). The direct character of the band gap, part (b), is represented by the black points, the indirect, by the blue ones. The red line presents a parabolic fit to the experimental data.

where $R(h\nu)$ is the reflectance of the sample measured *vs.* 100% reflectivity standard, $\alpha(h\nu)$ is the absorption coefficient and S stands for the scattering factor of the mixture, which practically is equal to the value of the pure diluent ($BaSO_4$) scattering factor. S may be regarded as a wavelength independent for a sufficiently large grain size (in comparison with the wavelength of incident light). The Kubelka-Munk formula is valid for the infinitely thick absorbing layer. Usually, to fulfil this condition, the layer thickness of approximately 3 mm is sufficient. However, in the case where the grains are much smaller than the wavelength of incident light, it may be necessary to prepare the sample as thick as 100 mm.[34] After the measurements, McLean analysis of the absorption edge was performed.[35]

The relation between the energy of the incident light ($h\nu$) and the f^{KM} in the vicinity of the absorption edge can be described using modified Tauc equation,[36, 37] Equation (4):

$$\left(f^{KM} h\nu\right)^{n/2} = A\left(h\nu - E_g\right) \quad (4)$$

In the above formula, a contribution from the phonon energy was neglected. A and n are parameters; where n depends on the transition character: $n = 1$ for the indirect transitions and $n = 4$ for the direct transitions. It was found that in the case of both $m$$BiVO_4$ and $m$$LaVO_4$ n equals 1, whereas $n = 4$ for the tetragonal, zircon-type phase.[8, 14] Thus, the monoclinic phases can be regarded as indirect band gap semiconductors and the tetragonal as direct ones. The Kubelka-Munk function plotted against incident light energy and the band gap dependence on the composition of the reaction mixture is presented in Fig. 4a. For pure $m$$LaVO_4$ the estimated value of the band gap (3.6 eV) is in a good agreement with measurements performed by Sun and co-workers (3.5 eV).[14] Introduction of 11.94 at. % of Bi^{3+} into pure $m$$LaVO_4$ results in the substantial increase in the band gap value, due to the phase transition from $m$$LaVO_4$ to $zt$$LaVO_4$. It means that $m$$LaVO_4$ should have narrower band gap than $zt$$LaVO_4$, contrary to the data from DFT calculations.[14] However, further introduction of Bi^{3+} into the $zt$$LaVO_4$ lattice results in a decrease in the band gap. Substitution of the La^{3+}cation, (characterized by the electronic configuration of Xe), with Bi^{3+} (p-block element) should reduce the width of the forbidden band due to the involvement of 6s states in the formation of the valence band.[19] Empty 6s states should result in a decrease of the valence band edge energy, while filled 6s levels should exert an opposite effect due to the effective mixing with oxygen 2p levels (Fig. 5). It is important to note that hard and weakly polarizable La^{3+} tends to form the highly ionic bonds, whereas much softer Bi^{3+} should provide a significant contribution to a covalently-bonded structure.[38] Specific interactions occurring between bismuth 6s levels and 2p levels of oxygen atoms lead to the significant increase in the valence band edge energy.[5]

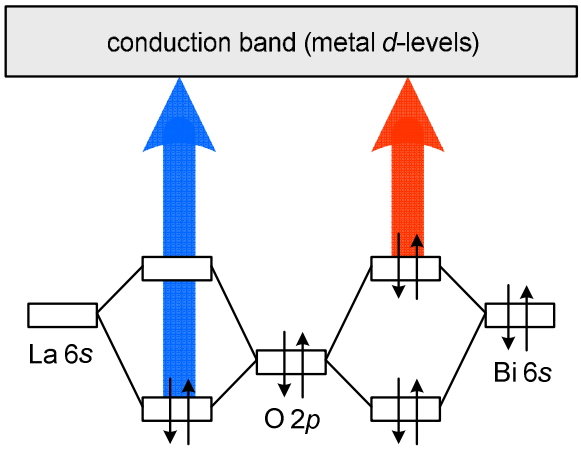

Fig. 5. The simplified qualitative band diagram and the nature of the fundamental transition in the lanthanum containing (blue) and bismuth-containing (red) oxide semiconductor. Adapted from ref.[39]

The existence of the two-phase region, ($zt$$BiVO_4$ with $m$$BiVO_4$, a small admixture of $m$$LaVO_4$ can be neglected), was confirmed for 92.86 at. % of Bi^{3+} by the XRD diffraction pattern and

SEM imaging (Fig. 3). In the UV-Vis reflectance spectrum of this sample the presence of two phases is manifested as two absorption steps. The McLean analysis was performed for both of them. The absorption spectrum was calculated twice. The first time for the indirect transition, second time for the direct one. The band gap value for the high-energy step was taken from the spectrum calculated for the direct transition and is in a good agreement with the value found for pure *zt*$BiVO_4$.[6] Since the low-energy absorption step originates from *m*$BiVO_4$, the band gap energy in this case was taken from the low-energy step in the spectrum calculated for the indirect one. The obtained value is very close to that one for the monoclinic phase. It means that the solubility of La^{3+} in the *m*$BiVO_4$ lattice is insubstantial.

The introduction of La^{3+} ions induces the phase transition (*m*$BiVO_4$ into *zt*$BiVO_4$). To determine the solubility changes that occur in the system within the range from 0 to 11.94 at. % of La^{3+}, the additional studies are necessary. The presence of residues of the *m*$LaVO_4$ phase does not influence the absorption edge of the solid solutions. On one hand, it contributes to the increase in the structural disorder and could be partially associated with the considerably higher absorption in the low-energy part of the spectrum (so called Urbach tail).[40] On the other hand, the presence of La^{3+}cations, (and the related energy levels), affects the part of the spectrum above the absorption edge, as the additional transitions are available.

In Fig. 4b it may be seen that the composition-band gap dependence can be well approximated by a parabola. Such a quadratic correlation of the band gap energy *vs.* the composition is a manifestation of the Van Vechten-Bergstresser model,[41] according to which, the band gap E_g of a solid solution of two semiconductors A and B can be expressed as a quadratic function of molar ratios of components, Equation (5):

$$E_g = E_B + (E_A - E_B - b)x + bx^2 \quad (5)$$

where x is the molar ratio of a component A and b is a *bowing factor*. Increasing value of the bowing factor indicates a significant lattice mismatch and/or differences in the electronic properties of the isovalent constituents.[42] The bowing factor calculated for the $BiVO_4$ – $LaVO_4$ system amounts to −1.41 ± 0.27 eV. The Van Vechten-Bergstresser model also allows to estimate the band gap energy values of two tetragonal phases that were not obtained using applied hydrothermal procedure: *zt*$BiVO_4$ and *zt*$LaVO_4$. The extrapolated E_g value for $LaVO_4$ amounts to approximately 3.9 eV, whereas, for $BiVO_4$ it is equal to 2.8 eV, which is in good agreement with the reported value of 2.9 eV.[6]

From Fig. 6a it may also be concluded that the absorption coefficient of the studied systems depends on the material composition. Such a dependence is presented in Fig. 6a. Two lowest values are observed for pure $LaVO_4$ and $BiVO_4$ phases (x = 0 and x = 1, respectively). With increasing x, the absorption coefficient increases and reaches its maximum at $x \approx 0.32$. Further increase in the Bi^{3+} content results in a slight decrease of the absorption coefficient which reaches local minimum at $x \approx 0.57$ and subsequent increase with the second maximum at $x \approx 0.76$. To explain such a behaviour, the role of the fundamental transition character should be considered. In the studied case pure phases show the indirect band gap, whereas solid solutions the direct one. For the indirect transitions, the absorption coefficient is usually much lower than for the direct transitions. Indeed, pure $LaVO_4$ and $BiVO_4$ phases exhibit the indirect band gaps, and their absorptivity (estimated from the reflectance) is lower than the one of the solid solutions. On the other hand, the absorption coefficient of the samples changes gradually with the composition which suggests other mechanism superimposed over the direct/indirect change of the fundamental transition.

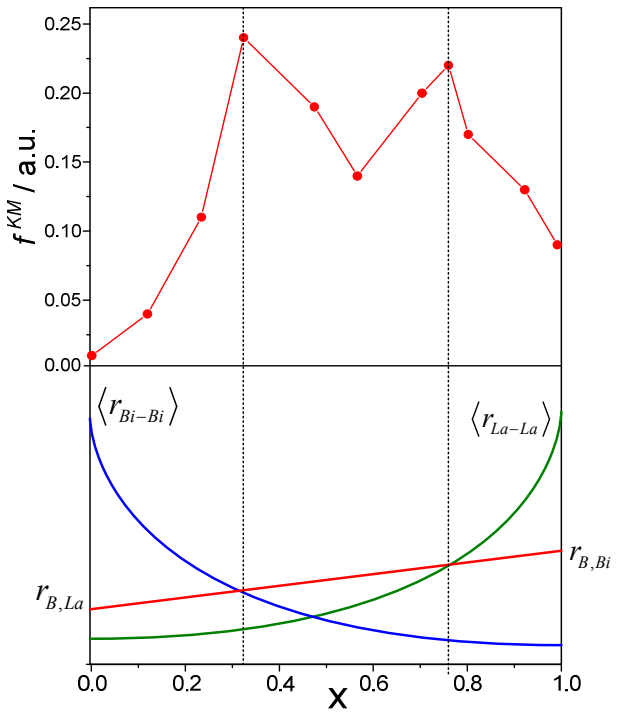

Fig. 6. The dependence of the maximum value of the Kubelka-Munk function in the studied systems as a function of bismuth content (a) and its correlation with the average distance between doping ions and the estimated exciton Bohr radius (b).

This can be associated with a local disorder of the lattice, as a random distribution of La^{3+} and Bi^{3+} results in the fluctuations of the local electric field. The characteristic length scale of these fluctuations (approximately 2 nm, which is comparable with the dimensions of the unit cell) is much shorter than the incident light wavelength. Therefore, the Anderson localization[43] of light cannot be directly responsible for the absorptivity changes.[44, 45] This subtle phenomenon, however, can be related to the polaritonic transport within the semiconductor particles. Then, the perturbation within the cationic sublattice should generate enough aperiodic distortion to increase slightly the absorption coefficient of the material. This process should be observed when the characteristic length of disorder is comparable with the Bohr radius of an exciton. The increasing concentration of dopant ions (Bi^{3+} in the case of $LaVO_4$ and La^{3+} in the case of $BiVO_4$) results in the decrease of the distance between them from infinity (for undoped crystals) to the average interaction distance in the lattice (for crystal composed only of "dopant ions" at the cationic sublattice) as schematically shown in Fig. 6b. At the same time, the expected value of Bohr radius changes gradually with changing the dielectric constant of the material and the effective masses of the charge carriers. In this case, two nearly symmetrical crossover point

should be found, where Bohr radius matches the average expected distance between the minority cations (dopants) in the lattice. These points may be associated with the local maxima of light absorption due to the exciton confinement as schematically shown in Fig. 6b.

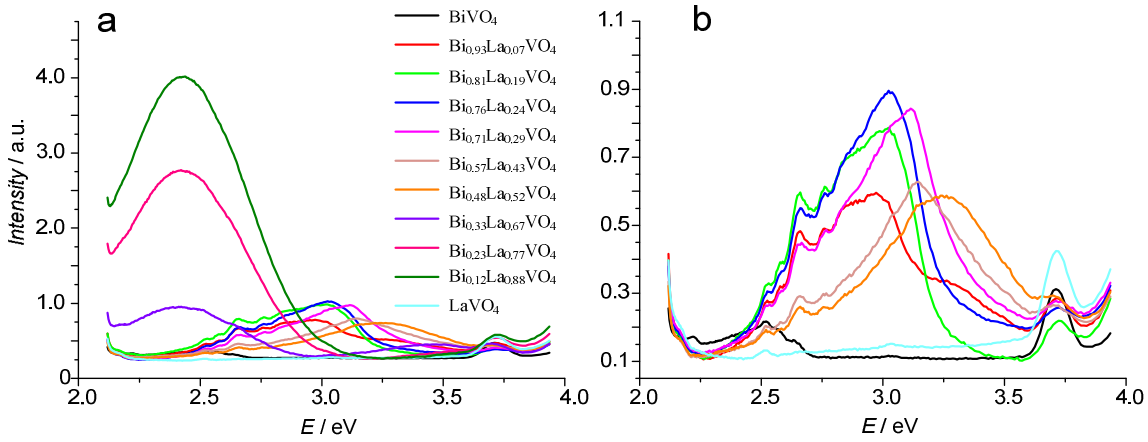

Fig. 7. The emission spectra of the synthesized powders suspended in deionized water; the samples were excited at 300 nm (a). The spectra with three most intensive signals removed (b).

It was already observed that numerous semiconductors show higher absorptivity near the absorption onset in the amorphous state than in the crystalline phase.[46, 47] However, the role of the structural disorder in the determination of optical properties is much less pronounced than in the case of the electrical properties.[48]

Apart from the band gap width and the absorption coefficient value, there is another important parameter which is necessary for full characterization of obtained materials – the conduction band edge potential. Its value was estimated using the Mott-Schottky analysis of the recorded EIS spectra. For the *n*-type semiconductor, the dependence of the space charge layer capacitance C on the electrode potential V may be formulated as follows,[49] Equation (6):

$$\frac{1}{C^2} = \frac{2}{\varepsilon\varepsilon_0 e N_D}\left(V - V_{fb} - \frac{k_B T}{e}\right) \quad (6)$$

where ε stands for the dielectric constant of the sample, ε_0 is the vacuum permittivity, e is the elementary charge, N_D – the donor density, V_{fb} – the flatband potential which may be regarded as the conduction band edge potential within 0.1 – 0.2 V accuracy, k_B – the Boltzmann constant and T – the temperature. Since the Mott-Schottky analysis is usually complicated due to the frequency dispersion, the constant phase element (CPE) was applied instead of the capacitor. Equation (7) expresses the impedance of the CPE:[50]

$$Z_{CPE} = \frac{1}{Q(j\omega)^{\alpha}} \quad (7)$$

where ω is the angular frequency and α is a constant, equal to 1 for the capacitor.

Since a simple equivalent circuit was applied, *i.e.* a resistor in series with the CPE, the capacitance can be easily calculated according to Equation (8):[50]

$$C = Q^{\frac{1}{\alpha}} R^{\frac{1-\alpha}{\alpha}} \quad (8)$$

First of all, the validity of the measurements was confirmed using the Kramers-Kronig transformation.[51, 52] Subsequently, the equivalent circuit was fitted to the spectra recorded at the different electrode potentials in the frequency range between 50 kHz and 10 Hz and a good fit was found (χ^2 approximately 10^{-5}). The detailed procedure of the Mott-Schottky analysis may be found in the authors' previous work.[53] The obtained values of the flat band potential are scattered within the range of −0.3 - 0 V *vs*. SHE (Standard Hydrogen Electrode) showing a negligible increase with the increase of the Bi^{3+} content. The obtained conduction band edge potential values are presented in Fig. 9b.

The contact potential difference (CPD) of the samples deposited onto a conductive substrate was also measured. Knowing the work function of the gold reference (WF_{Au} =5.1 eV),[54] the work function of the stainless steel tip (WF_{tip}) was calculated on the basis of the measurement of the CPD between the gold plate and the stainless steel tip, Equation (9):

$$WF_{tip} = WF_{Au} - CPD \quad (9)$$

Knowing the work function of the tip, the CPD between the sample and the tip was measured and the work function of the sample WF_{sample} was calculated, Equation (10):

$$WF_{sample} = WF_{tip} + CPD \quad (10)$$

The work function for the semiconductor can be associated with its Fermi level, which can be related – in the case of heavily doped *n*-type semiconductors – with the conduction band edge energy. Since the work function values were calculated *vs.* the vacuum level, they were converted to the standard hydrogen scale according to the Equation (11):

$$\frac{-WF_{sample} - 4.5\ \text{eV}}{e} = E_{sample} \quad (11)$$

where E_{sample} can be interpreted as the conduction band edge potential. All obtained values are scattered in the range of 0.8–1.1 V and do not change along with the composition of the samples (data not shown). The discrepancy, at the level of 1 V, between the values obtained from the EIS and CPD experiments arises due to the different conditions during both measurements (the electrochemical impedance spectroscopy experiment was performed in 0.1 M KCl, whereas the work function measurement was performed in the air) and different nature of the measured parameters, thus the aforementioned difference is fully acceptable. These experiments, however, confirm only mere dependence of the conduction band edge potential on the composition of the sample. This also indicates that the changes in the composition significantly affect the valence band energy. It demonstrates the role of the filled 6*s* states of bismuth which effectively interact with the oxygen 2*p* levels forming the upper part of the valence band.[39]

The emission spectroscopy was applied to investigate the electronic structure of the samples in more detail. The photoluminescence spectra of the prepared materials are presented in Fig. 7a. For clarity reasons, three strongest emission bands, for the samples characterized by the Bi^{3+} content in the range of 11.94 – 32.57 at. %, were removed from the plot shown inFig. 7b. The first conclusion that may be drawn is that there is a significant increase in the emission intensity for the $Bi_xLa_{1-x}VO_4$ (tetragonal, zircon-type structure) samples as compared to *m*$BiVO_4$ and *m*$LaVO_4$ themselves. It may be associated with the change of the band gap character from the indirect one, (in the monoclinic polymorphs), to the direct one, (in the tetragonal, zircon-type phase) and it confirms the assumed model used for the band gap calculations. It is also noteworthy that the emission bands visible at approximately 3 eV become blue-shifted when the content of La^{3+} in the reaction mixture is increased. It can be associated with a widening of the forbidden band with the increase in the La^{3+} concentration (Fig. 7b).

The emergence of the low-energy, high intensity signals in the samples characterized by the low Bi^{3+} concentration (i.e. from 11.94 to 32.57 at. %), can be attributed to the presence of the additional bismuth-related electronic states within the band gap. Since the very intense green emission slightly above 2.4 eV is observed, these states should be located approximately 2.4 eV below the conduction band edge. Closer inspection of the absorption spectra confirms the presence of such states (Fig. 8).

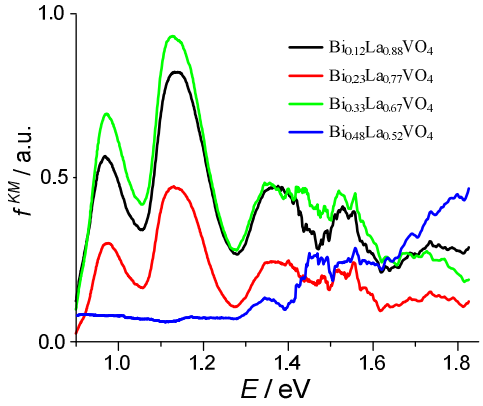

Fig. 8. The absorption spectra of the samples characterized by the low Bi^{3+} concentration (*i.e.* from 11.94 to 47.75 at. %).

For the samples exhibiting the intense green emission, (*i.e.* from 11.94 to 32.57 at. % of Bi^{3+}), three small absorption bands at 0.95, 1.15 and approximately 1.35 eV are visible, whereas the samples containing 47.75 at. % or more of Bi^{3+} show no absorption in this region. It also does not exhibit the intense luminescence in the green part of the emission spectrum. These absorption bands can be attributed to the transitions from the valence band to the states within the band gap. The higher Bi^{3+} concentration, the larger is the number of available, partially filled, states, introduced between the valence band edge and the top of the observed set of energy levels, which is located approximately 2.4 eV below the conduction band edge and does not change its energy. These states can be associated with the isolated bismuth ions.

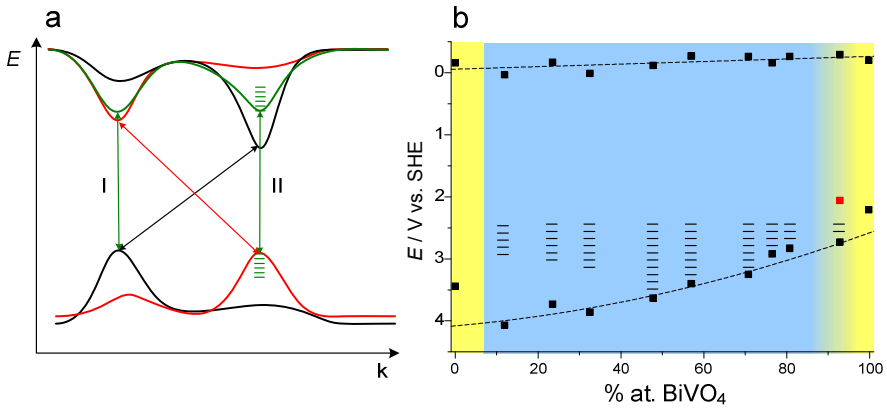

Fig. 9. A simplified picture of the postulated band structure of the examined materials in the wave vector space: $LaVO_4$ (red line), $BiVO_4$ (black line) and intermediate state – solid solution (green line). The arrows indicate possible transitions. In the case of solid solutions two different paths are available: direct, interband transition (I) and the deexcitation to the electronic states within the band gap (II) manifested as the intense green emission (a). A schematic representation of the electronic structure of studied materials. Yellow fields indicate the indirect character of the interband transition, the blue field – the direct type, whereas at 92.86 at. % of Bi^{3+} there are two phases: the Bi-rich one marked with the red square and the La–rich one marked with the black square. Two phase region is depicted as a shaded zone between the blue and the yellow areas. The black bars represent postulated electronic states within the energy gap (b).

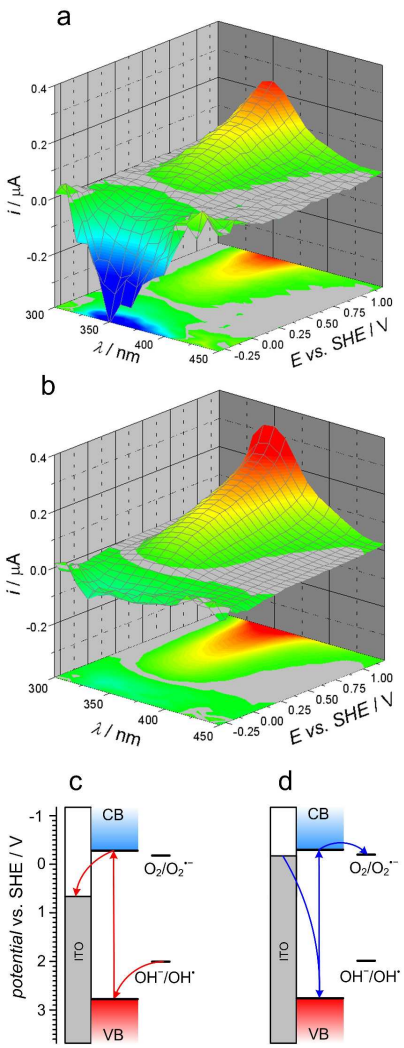

Fig. 10. The photocurrent amplitude as a function of the incident light wavelength and the photoelectrode potential for the sample containing 70.80 at. % of Bi^{3+} in the 0.1 M KNO_3 solution purged with oxygen (a) and with nitrogen (b) along with the mechanisms of the anodic (c) and cathodic (d) photocurrent generation. Formal reduction potential of oxygen and the hydroxyl ion was marked in the scheme based on ref.[55, 56]

The last step in the characterization of the obtained materials involved the investigation of the photoelectrochemical properties. The pulsed photocurrent action spectroscopy was used to follow the relative photocurrent generation efficiency, photocatalytic properties and photocurrent switching phenomena. It was found that the pure $LaVO_4$ phase is a poor photocurrent generator, yielding weak photocurrents (*ca.* 0.2 μA) in the UV range. Both the amplitude and the polarity of the photocurrent was found to be oxygen-independent. The same phenomenon was observed in the case of $Bi_xLa_{1-x}VO_4$ ($x \approx 0.12$). Increased bismuth content results in the increased photocurrent intensities, furthermore, in the presence of dissolved molecular oxygen, a photocurrent switching can be observed. This trend continues up to $x \approx 0.93$, where the pure $BiVO_4$ phase again generates only the anodic photocurrent irrespectively of the presence of oxygen. Fig. 10a and b show the photocurrent action spectra recorded at the different potential values in the 0.1 M KNO_3 solution purged with oxygen or nitrogen. Its amplitude decreases around 425 nm which is slightly below the value of the absorption edge measured with the reflectance spectroscopy, which may suggest the absorption within the Urbach tail. Depending on the electrode potential, either anodic or cathodic photocurrent is observed. Such a phenomenon is known as the Photoelectrochemical Photocurrent Switching Effect (the PEPS effect). [57-59] The switching potential is approximately equal to 0.2 V *vs*. SHE. When the electrolyte is purged with oxygen, below the switching potential, the intense cathodic photocurrent is observed. Removal of oxygen leads to the decrease in the photocurrent amplitude. Therefore, the cathodic reaction may be the one-electron reduction of molecular oxygen dissolved in the electrolyte. One should consider the one-electron redox reactions, since only one photon is needed to generate an electron–hole pair and induce the photocurrent flow. The mechanism of the switching phenomenon is summarized in Fig. 10c. The anodic photocurrent may be attributed to the one-electron oxidation of a hydroxyl group from the electrolyte (or adsorbed at the semiconductor surface) what is a typical process observed in the case of the wide band gap *n*-type semiconductors illuminated in the presence of aqueous electrolytes. In contrary, the $Bi_xLa_{1-x}VO_4$ phases show both the cathodic and anodic photocurrents in the presence of oxygen. This indicates that they can be of potential interest in the photocatalysis as oxygen activators.

Since the switching effect occurs around 0.2 V *vs*. SHE, the actual reduction potential of oxygen should be located close to this value, while the formal potential is equal to −0.16 V *vs*. SHE.[55] In fact, the real value depends on the concentration of oxygen dissolved in the electrolyte. Therefore, purging the solution with oxygen results in a shift in the reduction potential, towards more positive values. No photocorrosion is observed, since the hydroxyl ions can efficiently scavenge the holes. However, too negative electrode potential may result in the degradation of the material due to the redox processes involiving vanadium(V).

The switching effect was observed for the vast majority of the obtained samples with the exception of $BiVO_4$, $LaVO_4$ and the sample characterized by the 11.94 at. % of Bi^{3+} content. The change in the photocurrent direction from the anodic to cathodic (or vice versa) are due to the electrode polarization, was extensively described for the surface-modified semiconductors.[57] In the unmodified, *n*-type semiconductor, upward band bending prevents the electrons from the transition towards the electrolyte and thus, only the anodic photocurrent is observed.[60] In the presence of an efficient electron acceptor (*e.g.* molecular oxygen), the electrons from the conduction band could, in principle, tunnel through the potential barrier and reduce the electron acceptor in the electrolyte. However, the observed cathodic photocurrent intensity would be rather low. Therefore, all factors reducing the extent of the band bending should enhance the efficient generation of the cathodic photocurrent. The built-in-voltage V_{bi} (*i.e.* the potential drop between the semiconductor surface and the bulk) directly reflects the magnitude of the band bending and may be described as follows (12):[61]

$$V_{bi} = \frac{eN_D}{2\varepsilon_0\varepsilon}W^2 \qquad (12)$$

where ε stands for the dielectric constant of the sample, ε_0 is the vacuum permittivity, e is the elementary charge, N_D is the donor

density and *W* is the width of the depletion layer. Therefore, the decrease in the built-in-voltage may be realized by decreasing either the width of the depletion layer or the donor density. The former may be done by the reduction in the grain size of the powder. Indeed, for pure $BiVO_4$, 500 nm long crystals were obtained, whereas the introduction of La^{3+} ions resulted in the two-fold decrease of their dimensions. However, the latter factor may be of a higher importance. The introduction of Bi^{3+} into the $LaVO_4$ lattice (or the other way around) induces the formation of defects in the crystal structure (which is manifested for example as the presence of the Urbach tails). These defects could theoretically compensate the donor density and lower the position of the Fermi level, thus yielding rather compensated than the *n*-type semiconductor. Nonetheless, that is probably not the case, since the work function measurements indicate no significant influence of the Bi^{3+} ions concentration on the position of the Fermi level. The slopes on the Mott-Schottky plots recorded for each sample could in principle resolve this hypothesis, however, the actual surface area of the prepared electrodes is unknown just like individual dielectric constants. Despite the fact that the presented mechanism of the photocurrent switching still needs confirmation, described materials show prospective applications in construction of the optoelectronic logic devices.

Conclusion

The set of $Bi_xLa_{1-x}VO_4$ phases presents a simple chemical system, which can be tuned on different levels (crystal structure, electronic structure and quantum effects) by the simple cation substitution procedure. The materials are synthesized via the microwave-assisted hydrothermal route. For the pure $LaVO_4$ and $BiVO_4$ phases, monoclinic crystal structure was obtained, while the addition of at least 11.94 at. % of dopant ions leads to the phase transition from the monoclinic to the tetragonal, zircon-type structure. However, a small amount of the monoclinic phase still remains in most of the samples. Obtained results indicate the possibility to control the band gap energy and the valence band position via the substitution of the *d*-block with *p*-block metal cations in the lattice. The electrochemical impedance spectroscopy and the work function measurements indicate that the conduction band edge potential does not depend on the composition of the reaction mixture. Three samples with the lowest Bi^{3+} content (*i.e.* 11.94, 24.47 and 32.57 at. %) exhibit a very intense green emission which can be attributed to the presence of the electronic states within the band gap. This conclusion was also confirmed by the analysis of the absorption spectra. For higher Bi^{3+} concentration, the most intense emission peaks agree well with the band gap values obtained from the reflectance spectroscopy, however, some features corresponding to the green emission (and additional energy levels) are also visible. The photoelectrochemical characterization proves that the obtained solid solutions (from 24.47 to 92.86 at. % of Bi^{3+} concentration) exhibit the PEPS effect, which may be utilized in the construction of the optoelectronic logic devices in the nanoscale. Furthermore, the absorption coefficient can be finely tuned on the basis of the Anderson localization and the exciton confinement. All these features make the $Bi_xLa_{1-x}VO_4$ system a unique playground for both studying the basic phenomena in the solid state physics and for the development of novel materials for heterogeneous photocatalysis and optoelectronics.[62-64]

Acknowledgements

Authors thank Bela Szaciłowska for her assistance during preparation of the manuscript and Zbigniew Karkuszewski for discussions on Anderson localization. Financial support from National Science Centre (grant № UMO-2011/03/B/ST5/01495) and AGH University of Science and Technology (contract №11.11.180.509) is gratefully acknowledged.

Notes and references

[a] *AGH University of Science and Technology, Faculty of Non-Ferrous Metals, al. A. Mickiewicza 30, 30-059 Kraków, Poland; E-mail: szacilow@agh.edu.pl*
[b] *AGH University of Science and Technology, Faculty of Physics and Applied Computer Science, al. A. Mickiewicza 30, 30-059 Kraków, Poland*
[c] *Institute of Molecular Physics Polish Academy of Sciences, ul. M. Smoluchowskiego 17, 60-179 Poznań, Poland*
[d] *Jagiellonian University, Faculty of Chemistry, ul. Ingardena 3, 30-060 Kraków, Poland; E-mail: szacilow@chemia.uj.edu.pl*

1. A. Tücks and H. P. Beck, *J.Solid State Chem.*, 2005, **178**, 1145–1156.
2. A. Kudo and Y. Miseki, *Chem. Soc. Rev.*, 2008, **38**, 253-278.
3. M. M. Qurashi and W. H. Barnes, *Am. Mineral.*, 1952, **37**, 423-426.
4. R. S. Roth and J. L. Waring, *Am. Mineral.*, 1963, **48**, 1348-1356.
5. A. Walsh, Y. Yan, M. N. Huda, M. M. Al-Jassim and S.-H. Wei, *Chem. Mater.*, 2009, **21**, 547-551.
6. S. Tokunaga, H. Kato and A. Kudo, *Chem. Mater.*, 2001, **13**, 4624-4628.
7. A. Zhao, Z. Li and Z. Zou, *Phys. Chem. Chem. Phys*, 2011, **13**, 4746-4753.
8. K. Ding, B. Chen, Z. Fang and Y. Zhang, *Theor. Chem. Acc.*, 2013, **132**, 1352-1358.
9. H. Huang, D. Li, Q. Lin, W. Zhang, Y. Shao, Y. Chen, M. Su and X. Fu, *Environ. Sci. Technol.*, 2009, **43**, 4164–4168.
10. T. Hou, H. Yang, X. Fan and X. Zhang, *Catal. Lett.*, 2011, **141**, 1215–1218.
11. K.-T. Li and Z.-H. Chi, *Appl. Catal. A.*, 2001, **206**, 197–203.
12. J. Ma, Q. Wu and Y. Ding, *J. Nanopart. Res.*, 2008, **10**, 775–786.
13. Y. Oka, T. Yao and N. Yamamoto, *J. Solid State Chem.*, 2000, **152**, 486-491.
14. L. Sun, X. Zhao, Y. Li, P. Li, H. Sun, X. Cheng and W. Fan, *J. Appl. Phys.*, 2010, **108**, 0935191-09351910.
15. P. Parhi and V. Manivannan, *Solid State Sci.*, 2008, **10**, 1012-1018.
16. W. Fan, X. Song, Y. Bu, S. Sun and X. Zhao, *J. Phys. Chem. B*, 2006, **110**, 23247-23254.
17. B. Xie, G. Lu, Y. Wang, Y. Guo and Y. Guo, *Mater. Lett.*, 2011, **65** 240–243.
18. C.-J. Jia, L.-D. Sun, L.-P. You, X.-C. Jiang, F. Luo, Y.-C. Pang and C.-H. Yan, *J. Phys. Chem. B*, 2005, **109**, 3284-3290.
19. M. R. Dolgos, A. M. Paraskos, M. W. Stoltzfus, S. C. Yarnell and P. M. Woodward, *J. Solid State Chem.*, 2009, **182**, 1964–1971.
20. H. Xu, C. Wu, H. Li, J. Chu, G. Sun, Y. Xu and Y. Yan, *Appl. Surf. Sci.*, 2009, **256**, 597–602.
21. U. Mizutani, *Hume-Rothery Rules for Structurally Complex Alloy Phases*, Taylor & Francis, 2010.

22. L. Tian, Q. Sun, X. Xu, Y. Li, Y. Long and G. Zhu, *J. Solid State Chem.*, 2013, **200**, 123–127.
23. G. Liu, X. Duan, H. Li and H. Dong, *Mat. Chem. Phys.*, 2009, **115**, 165–171.
24. A. R. Lim, S. H. Choh and M. S. Jang, *J. Phys.: Condens. Matter*, 1995, **7**, 7309-7323.
25. A. Kudo, K. Ueda, H. Kato and I. Mikami, *Catal. Lett.*, 1998, **53**, 229-230.
26. H. M. Zhang, J. B. Liu, H. Wang, W. X. Zhang and H. Yan, *J. Nanopart. Res*, 2008, **10**, 767-774.
27. Y. Park, K. J. McDonald and K.-S. Choi, *Chem. Soc. Rev.*, 2013, **42**, 2321-2337.
28. C. Giacovazzo, *Fundamentals of Crystallography*, Oxford University Press, 2002.
29. L. Vegard, *Z. Phys.*, 1921, **5**, 17-26.
30. A. R. Denton and N. W. Ashcroft, *Phys. Rev. A*, 1991, **43**, 3161-3164.
31. M. J. Lambregts and S. Frank, *Talanta*, 2004, **62**, 627-630.
32. C. Y. Fong, W. Weber and J. C. Phillips, *Phys. Rev. B*, 1976, **14**, 5387-5391.
33. B.-T. Liou, S.-H. Yen and Y.-K. Kuo, *Appl. Phys. A*, 2005, **81**, 651-655.
34. G. Kortüm, *Reflectance spectroscopy Principles, Methods and Applications*, Springer-Verlag, Berlin Heidelberg New York, 1969.
35. T. P. McLean, in *Progress in Semiconductors*, ed. A. F. Gibson, Heywood & Company Ltd., London, 1960, vol. 5, ch. 2.
36. J. Tauc, *Mater. Res. Bull.*, 1968, **3**, 37-46.
37. J. I. Pankove, *Optical Processes in Semiconductors*, Prentience-Hall Inc., New Jersey, 1971.
38. R. G. Pearson, *J. Am. Chem. Soc.*, 1963, **85**, 3533-3539.
39. K. Sayama, in *Photoelectrochemical hydrogen production*, eds. R. Van der Krol and M. Graetzel, Springer, New York, 2012.
40. A. Podborska, B. Gaweł, Ł. Pietrzak, I. B. Szymańska, J. K. Jeszka, W. Łasocha and K. Szaciłowski, *J. Phys. Chem. C*, 2009, **113**, 6774-6784.
41. J. A. Van Vechten and T. K. Bergstresser, *Phys. Rev. B*, 1970, **1**, 3351-3358.
42. S.-H. Wei, S. B. Zhang and A. Zunger, *J. Appl. Phys.*, 2000, **87**, 1304-1311.
43. P. W. Anderson, *Phys. Rev.*, 1958, **109**, 1492-1505.
44. M. Störzer, P. Gross, C. M. Aegerter and G. MAret, *Phys. Rev. Lett.*, 2006, **96**, 063904.
45. J. Gómez Rivas, R. Sprik and A. Lagedijk, *Phys. Rev. E*, 2001, **63**, 046613.
46. J. Tauc, in *Amorphous and liquid semiconductors*, ed. J. Tauc, Plenum Press, London, 1974.
47. R. A. Street, *Hydrogenated amorphous silicon*, Cambridge University Press, Cambridge, 1991.
48. K. Tanaka and K. Shimakawa, *Amorphous chalcogenice semiconductors and related materials*, Springer Science + BUsiness Madia, LLC, New York, 2011.
49. W. P. Gomes and D. Vanmaekelbergh, *Electrochim. Acta*, 1996, **41**, 967-973.
50. M. A. Orazem and B. Tribollet, *Electrochemical impedance spectroscopy*, John Wiley & Sons, Hoboken, New Jersey., 2008.
51. B. A. Boukamp, *Solid State Ionics*, 2004, **169**, 65-73.
52. B. A. Boukamp, *J. Electrochem. Soc.* , 1995, **142**, 1885-1894.
53. P. Kwolek and K. Szaciłowski, *Electrochim. Acta*, 2013, **104**, 448-453.
54. H. B. Michaelson, *J. Appl. Phys.*, 1977, **48**, 4729-4733.
55. D. T. Sawyer and J. S. Valentine, *Acc. Chem. Res.*, 1981, **14**, 393-400.
56. P. Wardman, *J. Phys. Chem. Ref. Data*, 1989, **18**, 1637-1755.
57. S. Gawęda, R. Kowalik, P. Kwolek, W. Macyk, J. Mech, M. Oszajca, A. Podborska and K. Szaciłowski, *Isr. J. Chem.*, 2011, **51**, 36-55.
58. K. Szaciłowski and W. Macyk, *Comp. Rend. Chimie*, 2006, **9**, 315-324.
59. K. Szaciłowski and W. Macyk, *Chimia*, 2007, **61**, 831-834.
60. R. Memming, *Semiconductor electrochemistry*, Wiley-VCH, Weinheim, 2001.
61. M. X. Tan, P. E. Laibinis, S. T. Nguyen, J. M. Kesselman, C. E. Stanton and N. S. Lewis, *Prog. Inorg. Chem.*, 1994, **41**, 21-144.
62. S. Gawęda, A. Podborska, W. Macyk and K. Szaciłowski, *Nanoscale*, 2009, **1**, 299-316.
63. T. Zhai, X. Fang, L. Li, Y. Bando and D. Goldberg, *Nanoscale*, 2010, **2**, 168-187.
64. J. M. Macak, T. Kohoutek, L. Wang and R. Beranek, *Nanoscale*, 2013, **5**, 9541-9545.

TOC text

Bismuth-lanthanum vanadate solid solutions of tunable electronic and optical properties are promising materials for novel optoelectronic devices.

TOC graphics